

1 Thermodynamic Properties and Transport Coefficients of Two Temperature 2 Teflon Vapour Plasma for Ablation Controlled Discharge Applications

3 Haiyan Wang^{1, (a)}, Weizong Wang^{2, (a),*}, Joseph D Yan³, Haiyang Qi¹, Jinyue Geng⁴ and Yaowu Wu⁴

4 1. Pinggao Group Co. Ltd., Pingdingshan City, Henan 467001, China

5 2. Qian Xuesen Laboratory of Space Technology, China Academy of Space Technology, Beijing 100094,
6 China

7 3. Department of Electrical Engineering and Electronics, The University of Liverpool, Liverpool L69 3GJ,
8 UK

9 4. Beijing Institute of Control Engineering, China Academy of Space Technology, Beijing 100094, China

10 E-mail: wangweizong@gmail.com

11 * Author to whom any correspondence should be addressed.

12 Current address: University of Antwerp, BE-2610 Wilrijk-Antwerp, Belgium.

13 (a) These authors contributed equally to this work

14 **Abstract:** Ablation-controlled plasmas have been used in a range of technical applications where local
15 thermodynamic equilibrium (LTE) is often violated near the wall due to strong cooling effect caused by
16 ablation of the wall materials. The thermodynamic and transport properties of ablated polytetrafluoroethylene
17 (PTFE) vapor, which determine the flowing plasma behavior in such applications, are calculated based on a
18 two-temperature model at atmospheric pressure. To our knowledge, no data for PTFE have been reported in
19 literature. The species composition and thermodynamic properties are numerically determined using the
20 two-temperature Saha equation and Guldberg-Waage equation according to van de Sanden *et al.*'s derivation.
21 The transport coefficients including diffusion coefficient, viscosity, thermal conductivity, and electrical
22 conductivity are calculated with most recent collision interaction potentials using Devoto's electron and heavy
23 particle decoupling approach but expanded to the third-order approximation (second-order for viscosity) in the
24 frame of Chapman–Enskog's method. Results are computed for different degrees of thermal non-equilibrium,
25 i.e. the ratio of electron to heavy particle temperatures, from 1 to 10, with the electron temperature ranging
26 from 300 to 40,000 K. Plasma transport properties in LTE state obtained from the present work are compared
27 with existing published results and causes for the discrepancy analyzed. The two-temperature plasma
28 properties calculated in the present work enable the modelling of wall ablation controlled plasma processes.

29 **Keywords:** Wall ablation; Teflon; non-equilibrium plasma; two temperature model; thermodynamic
30 properties; transport coefficients

31 **Submitted to** Journal of Physics D: Applied Physics

32

33

34

1 **1. Introduction**

2 Ablation-controlled plasmas are widely used in technologic applications such as high current switching
3 [1]-[3] soft x-ray generation [4], pulsed plasma thrusters (PPT) [5]-[7], electrothermal-chemical (ETC)
4 launching [8]-[9], and laser ablation [10]-[11]. Polytetrafluoroethylene (Teflon, PTFE) as a polymer material
5 has been used in most of these applications. The compound-materials vaporize when subjected to strong
6 heating from the high power plasma and as a result a vapor mass flow is injected into the plasma. Thus the
7 ablated vapor becomes part of the plasma and significantly influences the discharge process and plasma
8 parameters such as temperature, velocity and pressure. To improve the process efficiency, a
9 Magnetohydrodynamics (MHD) model had been developed and applied to investigate the ablation
10 characteristics of heated compound-materials interacting with discharging plasma [1]-[3].

11 The assumption of local thermodynamic equilibrium (LTE), which is used in the MHD model of ablation
12 dominated arcs at high current, is no longer valid as a result of large temperature gradient (existing near a cold
13 wall or when cold vapor is injected in the plasma) or insufficient electron number density to achieve efficient
14 energy exchange between electrons and heavy species [12]. Under such circumstances, while electrons and
15 heavy species are able to maintain their Maxwellian velocity distribution functions, the mean kinetic energy of
16 electrons can be much higher than that of heavy particles. A two-temperature MHD model would thus be
17 required, which has to be based on non-equilibrium thermodynamic and transport properties of the plasma
18 [13]-[14]. The description of the state of a two-temperature plasma maintained in polymer vapor involves
19 complex microscopic processes such as dissociation reactions, excitation into different types of discrete
20 energy levels (rotational, vibrational and electronic), and ionization of different atomic species, etc. A
21 common approach to render the problem attackable is to use the principle of local chemical equilibrium (LCE)
22 with different electron (T_e) and heavy-particle (T_h) temperatures [15]-[16].

23 Existing work is all limited to plasmas under LTE conditions, only for pure CF_4 , C_2F_6 as well as ablated
24 vapour of PTFE $(C_2F_4)_m$ [1],[18]-[19]. To our knowledge, there has been no published work so far on the
25 thermodynamic properties and transport coefficients of two-temperature PTFE plasma. To fill this gap, the
26 two-temperature plasma properties of evaporated Teflon are calculated in the present work. Results are
27 presented and discussed mainly over an electron temperature range of 300 K to 40,000 K although
28 calculations have been carried out under different pressures and higher electron temperature up to 60,000 K.
29 The most recent cross-section data with highest accuracy specified in literature have been used in the
30 evaluation of the collision integrals. Results in LTE as an extreme case in the present work are compared with
31 published data and the possible reasons for the discrepancies analysed.

32

33 **2. Mathematical Models**

34 **2.1 Determination of plasma composition**

35 The first step in the calculation of the thermodynamic properties and transport coefficients of the non-LTE

1 plasma is to determine the species composition [20]-[21]. The plasma of ablated PTFE vapor has different
 2 species at different temperature. Considering the possible temperature range, a total of 24 different species,
 3 including atoms, ions and molecular radicals as well as electrons, are included in the calculation: C_2F_4 , C_2F_2 ,
 4 CF_4 , CF_3 , CF_2 , CF , C_5 , C_4 , C_3 , C_2 , C , F_2 , F , CF_3^+ , CF_2^+ , CF^+ , C^+ , F^+ , F^- , C^{2+} , F^{2+} , C^{3+} , F^{3+} . Other molecular ions
 5 are excluded because of their low density and negligible effect on the thermodynamic and transport properties.
 6 A total of 21 independent reactions are taken into account (table 1) and described by the mass action law, i.e.
 7 Saha's equation for ionization and Gulberg–Waage's law for dissociation reactions.

8 **Table 1 List of reactions considered in the present work.**

Number	Chemical reaction	Number	Chemical reaction
1	$C_2F_4 \rightleftharpoons C_2F_2 + F_2$	12	$F \rightleftharpoons F + e$
2	$C_2F_2 \rightleftharpoons CF_2 + C$	13	$F \rightleftharpoons F^+ + e$
3	$CF_4 \rightleftharpoons CF_3 + F$	14	$C \rightleftharpoons C^+ + e$
4	$CF_3 \rightleftharpoons CF_2 + F$	15	$F^+ \rightleftharpoons F^{2+} + e$
5	$CF_2 \rightleftharpoons CF + F$	16	$C^+ \rightleftharpoons C^{2+} + e$
6	$CF \rightleftharpoons C + F$	17	$F^{2+} \rightleftharpoons F^{3+} + e$
7	$C_5 \rightleftharpoons C_4 + C$	18	$C^{2+} \rightleftharpoons C^{3+} + e$
8	$C_4 \rightleftharpoons C_3 + C$	19	$CF_3 \rightleftharpoons CF_3^+ + e$
9	$C_3 \rightleftharpoons C_2 + C$	20	$CF_2 \rightleftharpoons CF_2^+ + e$
10	$C_2 \rightleftharpoons C + C$	21	$CF \rightleftharpoons CF^+ + e$
11	$F_2 \rightleftharpoons F + F$		

9
 10 For two-temperature plasmas, there exist two forms of the mass action law, represented by Potapov's
 11 method [24] and Van de Sanden et al.'s method [25]. Our previous work for two temperature SF_6 plasma has
 12 shown that the difference in the two Saha equations leads to significant discrepancy in species composition
 13 and hence the plasma properties [26]. For example, Potapov's approach leads to larger variation in species
 14 concentration and plasma properties at high non-equilibrium degree (T_e/T_h), especially the specific heat at
 15 constant pressure and thermal conductivity both of which are closely related to the energy associated with
 16 chemical reactions. To the best of our knowledge, there has been no experimental evidence that can be used to
 17 justify the conditions under which the approaches are valid. Based on the argument that in the extreme case of
 18 very high or very low electron number density, laws governing dissociation and ionization must not depend on
 19 $\theta = T_e/T_h$, Van de Sanden et al.'s approach has been recommended by Gleizes et al through a comparative
 20 study of the composition of a two-temperature SF_6 plasmas based on the two approaches[27]. In view of the
 21 argument in [27] and also the fact that Van de Sanden's approach has been widely cited in literature as a
 22 reference case for chemical equilibrium calculations [28]. This approach is also adopted in the present work.
 23 The Guldberg–Waage equation and generalized Saha law are expressed for dissociation reaction as
 24 $ab \leftrightarrow a + b$ where equilibrium is controlled by the heavy species kinetic temperature T_h , and for ionization
 25 as $a^{r+} \leftrightarrow a^{(r+1)+} + e$ which is controlled by the electron temperature.

$$1 \quad \frac{n_a n_b}{n_{ab}} = \frac{Q_a Q_b}{Q_{ab}} \left[\frac{2\pi k T_h}{h^2} \right]^{3/2} \left[\frac{m_a m_b}{m_{ab}} \right]^{3/2} \exp\left[-\frac{E_d}{k T_{ex}}\right] \quad (1)$$

$$2 \quad n_e \left[\frac{n_{r+1}}{n_r} \right] = 2 \left[\frac{Q_{r+1}}{Q_r} \right] \left[\frac{2m_e \pi k T_e}{h^2} \right]^{3/2} \exp\left[-\frac{E_{I,r+1} - \delta E_{I,r+1}}{k T_{ex}}\right] \quad (2)$$

3 where Q is the internal partition function. $E_{I,r+1}$ and E_d are the ionization energy and dissociation energy,
 4 respectively; k and h are the Boltzmann constant and Planck constant. The subscript r represents r -times
 5 ionized species or molecules. ab , a , b and e denote, respectively, the reactant, two products of the dissociation
 6 reaction and electrons, n_i and m_i are the number density and mass of specie i , and T_{ex} is the excitation temperature
 7 of species a^{r+} ionization. $\delta E_{I,r+1}$ is the lowering of the ionization energy when taking into account the shielding effects
 8 of both ions and electrons in the calculation of the Debye Length [26]. The choice of this excitation temperature
 9 has been discussed widely in previous studies and is still subjected to debate [26]. The authors have taken the
 10 argument that the heavy particle temperature T_h is responsible for dissociation reactions and the electron
 11 temperature T_e controls the ionization reactions. The species partition functions are then computed according
 12 to the mathematical model presented in [20].

13 Fundamental data associated with the electronic energy levels of neutral atoms and atomic ions for the
 14 evaluation of their partition functions are taken from the NIST database [29]. The ionization and dissociation
 15 energies have also been taken from [29]. The rotational and vibrational constants for the calculation of
 16 partition functions of molecules are taken from JANAF tables [30].

17 In addition to the law of mass action (Saha's law and Gulberg–Waage's law) as detailed above, the
 18 calculation of the species composition of the two temperature plasma requires additional three equations to
 19 close the system of equations. They are based on conservation of chemical elements, Dalton's Law for
 20 equation of state, and electrical quasi-neutrality. The complete set of equations are solved using the Newton–
 21 Raphson method to obtain well converged results.

22 **2.2 Determination of thermodynamic properties**

23 With the knowledge of plasma composition, the thermodynamic properties can be calculated based on
 24 classical theory of statistical mechanics. The standard thermodynamic relationships used in the work of Wang
 25 et al [20],[26] are used, as detailed below for information.

26 (a) Mass density

$$27 \quad \rho = \sum_i^w n_i m_i \quad (3)$$

28 where w is the number of species with a value of 24 for the plasma under study, n_i the number density and m_i
 29 the mass per particle, of species i .

30 (b) Specific enthalpy

31 The computed specific enthalpy takes into account the translational, reactional and contributions by
 32 excitation of the internal discrete states. Since electronic excitation is governed by electron temperature and

1 molecular rotation and vibration of species governed by heavy particle temperature, the contributions have to
 2 be accounted for separately as given below:

3 For electrons,

$$4 \quad h_e = \frac{5}{2} \frac{k}{\rho} n_e T_e \quad (4)$$

5 For monatomic species,

$$6 \quad h_i = \frac{5}{2} \frac{k}{\rho} n_i T_h + \frac{1}{\rho} n_i E_i + \frac{k}{\rho} n_i (T_e^2 \frac{\partial \ln Q_i^{el}}{\partial T_e}) \quad (5)$$

7 where Q_i^{el} is the electronic partition function of specie i and E_i is the standard formation energy of species i .

8 For molecular species,

$$9 \quad h_i = \frac{5}{2} \frac{k}{\rho} n_i T_h + \frac{1}{\rho} n_i E_i + \frac{k}{\rho} n_i (T_e^2 \frac{\partial \ln Q_i^{el}}{\partial T_e} + T_h^2 \frac{\partial \ln(Q_i^{rot} Q_i^{vib})}{\partial T_h}) \quad (6)$$

10 where Q_i^{rot} and Q_i^{vib} are the rotational and vibrational partition function of specie i .

11 The total specific enthalpy and heavy particles specific enthalpy are

$$12 \quad h = \sum_i^w h_i$$

$$13 \quad h_h = \sum_{i \neq e}^w h_i \quad (7)$$

14 (c) Specific heat

15 The specific heat for electrons and heavy particles as well as total specific heat at constant pressure and
 16 constant non-equilibrium degree are obtained below based on our previous deviation [26]:

$$17 \quad CP_e = \frac{\partial h_e}{\partial T_e} + \frac{\partial h_e}{\partial T_h} \frac{1}{\theta} \quad (8)$$

$$18 \quad CP_h = \frac{\partial h_h}{\partial T_e} \theta + \frac{\partial h_h}{\partial T_h} \quad (9)$$

$$19 \quad CP_t = \frac{\partial h}{\partial T_e} \theta + \frac{\partial h}{\partial T_h} \quad (10)$$

20 2.3 Determination of Transport Coefficients

21 Transport properties, namely diffusion coefficients, electrical conductivity, thermal conductivities and
 22 viscosity, are calculated using the classical Chapman–Enskog method [31]-[33], where the velocity
 23 distribution functions of different species can be expended into a Maxwellian distribution function and a
 24 first-order perturbation function. The perturbation is expressed in a series of Sonnie polynomials, thus giving a
 25 system of linear equations which can then be solved to obtain different transport coefficients [31]. For

1 partially ionized plasmas, two approaches have been used extensively to calculate the two-temperature
 2 transport properties in which local chemical equilibrium is satisfied, i.e. (1) a simplified theory proposed by
 3 Devoto [34] and Bonnefoi [35] which neglects the collisional coupling between heavy species and electrons,
 4 and, (2) the method proposed by Rat et al [36] which considers the coupling. For LTE plasmas, results
 5 obtained with the simplified theory are in good agreement with those of the non-simplified theory; for
 6 Non-LTE plasmas, consideration of coupling between heavy species and electrons results in more equations to
 7 be solved, and thus computationally more expensive, as compared with the simplified theory of Devoto [34]
 8 and Bonnefoi [35]. Furthermore, the computed transport properties considering coupling do not show
 9 significant difference from those computed excluding the effects of coupling, except for certain ordinary
 10 diffusion coefficients as shown by the work of Colombo et al. [37]. The simplified approach of Devoto [34]
 11 and Bonnefoi [35] is therefore used in the present work. It is assumed that change in the perturbation function
 12 in electrons is greater than that of heavy species in interactions involving both types of particles. A third-order
 13 approximation is used for the calculation of transport properties, except for viscosity for which the
 14 second-order approximation has been adopted and can ensure enough high calculation accuracy.

15 Of the transport coefficients in a two-temperature plasma, special attention should be paid to the thermal
 16 conductivity which depends not only on the translation of the particles but also on processes involving internal
 17 energy state changes and chemical reactions. Chemical reactions absorb or release energy, leading to
 18 additional heat flux which is represented by a reactive thermal conductivity component λ_r . The reactive
 19 thermal conductivity components of electrons and heavy particles are separately determined by an expression
 20 derived through reactive heat flux treating electrons and heavy particles separately [38]-[39].

$$\begin{aligned}
 21 \quad \lambda_{re} &= \left[\sum_{r=1}^v \Delta h_r \frac{n}{\rho k T_h} \sum_{j=1}^w \frac{T_h}{T_j} m_j D_{rj}^a \frac{\partial p_j}{\partial T_e} \right] \\
 22 \quad \lambda_{rh} &= \left[\sum_{r=1}^v \Delta h_r \frac{n}{\rho k T_h} \sum_{j=1}^w \frac{T_h}{T_j} m_j D_{rj}^a \frac{\partial p_j}{\partial T_h} \right] \tag{11}
 \end{aligned}$$

23 where n , v and Δh_r are, respectively, total number density of all species, number of chemical reactions and
 24 reaction enthalpy change of reaction r . P_j is the partial pressure of specie j . D_{rj}^a is the ambipolar diffusion
 25 coefficient defined in terms of ordinary diffusion coefficients [38].

$$26 \quad D_{ij}^a = D_{ij}^m + \frac{\alpha_i}{\beta} \sum_s Z_s D_{sj}^m \tag{12}$$

27 where coefficients α_i and β are given by

$$28 \quad \alpha_i = \sum_j \frac{m_j n_j Z_j D_{ij}^m}{T_j}$$

$$\beta = \sum_i Z_i \sum_j \frac{m_j n_j Z_j D_{ij}^m}{T_j} \quad (13)$$

and Z_s and Z_i are the charges number for specie s and i , respectively.

The knowledge of ordinary diffusion coefficients is a prerequisite to (12) and can be determined following the framework of Hirschfelder *et al.*[31].

$$D_{ij}^m = \frac{F^{ji} - F^{ii}}{m_j |F|} \quad (14)$$

where F^{ji} are the cofactors of the matrix F whose elements are defined as

$$F_{ij} = \frac{1}{\rho} \left[\frac{n_i}{D_{ij}^b} + \sum_{l \neq i} \frac{n_l m_j}{m_l D_{il}^b} \right] (1 - \delta_{ij}) \quad (15)$$

The binary diffusion coefficient is evaluated based on the derivation of two temperature transport properties, as reported by Ramshaw [40]-[41].

$$D_{ij}^b = \frac{3k^2 T_i T_j}{16P \mu_{ij} T_{ij}^* \Omega_{ij}^{(1,1)}} \quad (16)$$

where Ω_{ij} is the collision integrals. μ_{ij} and T_{ij}^* are, respectively, the reduced mass and the reduced temperature of colliding molecules i and j , which are defined as

$$\frac{1}{\mu_{ij}} = \frac{1}{m_i} + \frac{1}{m_j} \quad (17)$$

$$T_{ij}^* = \frac{(m_i T_j + m_j T_i)}{m_i + m_j} \quad (18)$$

The partial derivative of partial pressure with respect to T_h and T_e can be determined by differentiating the partial pressure equation (from Dalton's law) with respect to T_h and T_e which are treated as independent variables. When the thermal conductivity is evaluated in terms of heavy particle temperature gradient, a total reactive thermal conductivity can be defined as

$$\lambda_{r e a c} = \lambda \theta_r \frac{\lambda}{\lambda} \quad (19)$$

The presence of an internal degree of energy freedom affects the heat flux vector and gives rise to an internal thermal conductivity component λ_{in} . It is derived using the Hirschfelder–Eucken approximation [42]:

$$\lambda_{\text{int}} = \sum_{i \neq e}^w x_i D_{ii}^b k (C_{pi} / R - 2.5) \left(\sum_{j \neq e}^w \frac{x_j D_{ij}^b}{x_i D_{ij}^b} \right)^{-1} \quad (20)$$

where C_{pi} is the specific heat at constant pressure of species i , D_{ii}^b and D_{ij}^b , respectively, the self-diffusion coefficient and binary diffusion coefficient between species i and j . R , P , x_i , and w denote, respectively, the molar gas constant, total pressure, mole fraction of species i , and the total number of species.

The total thermal conductivities for electrons and heavy particles, designated as λ_e and λ_h , can be expressed, respectively, as

$$\lambda_e = \lambda_{tre} + \lambda_{re}$$

and

$$\lambda_h = \lambda_{trh} + \lambda_{rh} + \lambda_{in} \quad (21)$$

where λ_{tre} and λ_{trh} are the translational thermal conductivity components of electrons and heavy particles.

2.4 Evaluation of collision integrals

The transport coefficients rely on collision integrals representing the effect of interaction potential between two species i and j . They are statistical averages, over a Maxwellian distribution, of the collision cross-sections for pairs of species and defined as [31]-[33]:

$$\Omega_{ij}^{(l,s)} = \sqrt{\frac{kT_{ij}^*}{2\pi\mu_{ij}}} \int_0^\infty \exp(-\gamma_{ij}^2) \gamma_{ij}^{2s+3} Q_{ij}^l(g) d\gamma_{ij} \quad (22)$$

where k is Boltzmann constant, T_{ij}^* the effective temperature of the colliding particles, μ_{ij} the reduced mass and γ_{ij} is the reduced initial speed of species i and j , given by

$$\gamma_{ij} = \sqrt{\frac{\mu_{ij}}{2kT_{ij}^*}} g_{ij} \quad (23)$$

where g_{ij} is the initial relative speed of the species, and $Q_{ij}^l(g)$ is the transport collision cross sections.

Knowledge of transport cross sections is a prerequisite to the evaluation of the collision integrals as shown in equation (22). The following methods are utilized to obtain the transport cross sections.

2.4.1 Elastic transport cross section

A. Analytical interaction potential

The transport cross sections $Q_{ij}^l(g)$ can be obtained by integration as shown below once the interaction potential is known:

1

$$Q_{ij}^l(g) = 2\pi \int_0^\infty (1 - \cos^l \chi) b db \quad (24)$$

3 where χ is the angle by which the molecules are deflected in the centre of gravity coordinate system, defined
4 by

$$\chi = \pi - 2b \int_{r_m}^\infty \frac{dr / r^2}{\sqrt{1 - \left[\varphi_{ij}(r) / \frac{1}{2} \mu_{ij} g_{ij}^2 \right] - b^2 / r^2}}, \quad (25)$$

6 and b is the impact parameter. The term r_m is the outermost root of the equation and $\varphi_{ij}(r)$ is the potential
7 energy of interaction between the colliding particles, satisfying

$$1 - \frac{\varphi_{ij}(r)}{\frac{1}{2} \mu_{ij} g_{ij}^2} - \frac{b^2}{r_m^2} = 0 \quad (26)$$

9

10 The analytical forms for the interaction potential $\varphi_{ij}(r)$ of PTFE species used in this work contain
11 HFD-B Like potential, Hulburt–Hirschfelder potential, Murrell–Sorbie potential, Exponential Repulsive
12 potential, Phenomenological potential, and Polarization potential. Details can be found in our most recent
13 compilation [18].

14 *B. Numerical integration of elastic collision differential cross sections*

15 These transport cross sections for electron-neutral species interactions are obtained by numerically
16 integrating the differential cross sections $\frac{d\sigma}{d\Omega}$ over all scattering angles as a function of the interaction
17 energy as follows.

$$Q^l(E) = 2\pi \int_0^\pi \frac{d\sigma}{d\Omega} \sin \theta (1 - \cos \theta^l) d\theta \quad (27)$$

19 where E is the total kinetic energy of the colliding particles, dominated by the electron energy. Differential
20 cross sections $\frac{d\sigma}{d\Omega}$ are determined by either experiment or through theoretical computation. When differential
21 cross sections are not available, the techniques recommended by Laricchiuta et al. [43] are used to determine
22 the transport cross sections. The ratio $Q^2(E)/Q^1(E)$ and $Q^3(E)/Q^1(E)$ are evaluated from the known $Q^1(E)/Q^0(E)$
23 assuming a model angular dependence of the differential cross section:

$$\frac{1}{(1 - C(E) \cos \theta)^2} \quad (28)$$

25 where C is here an adjustable parameter as a function of the electron energy, determined from the

1 $Q^l(E)/Q^0(E)$ ratio. When the $Q^0(E)$ cross section is not known, the value of C can be fixed according to Born
 2 scattering for a Coulomb screened potential

$$3 \quad \frac{1}{(1+2\eta)^2} \quad \text{with} \quad \eta = 10.9Z^{2/3} / E \quad (29)$$

4 **2.4.2 Inelastic resonant charge-exchange cross section**

5 For neutral-ion interactions, two types of processes should be taken into account; purely elastic collisions
 6 and the inelastic resonant charge-exchange process. For odd values of l ($l = 1$ and 3), inelastic resonant
 7 charge-exchange process plays an important role in determining the collision integrals $\Omega_{ij}^{(l,s)}$. In order to
 8 numerically evaluate the charge-exchange collision integrals, it is necessary to know the charge-exchange
 9 cross section. For interactions between a parent atom or molecule X and its ion X^- or X^+ , particularly for
 10 high collision energies, the transport cross section can be evaluated using

$$11 \quad Q^l(g) = 2Q_{ex} \quad (30)$$

12 where the charge-transfer cross section is approximated in the form

$$13 \quad Q_{ex} = (A - B \ln E)^2 \quad (31)$$

14 where E is the kinetic energy of the colliding particles. The constants A and B can be obtained from
 15 experimental data or theoretical calculations.

16 For interactions in which charge exchange occurs collision integrals with odd value of l , including both
 17 elastic and inelastic processes, can be estimated by an empirical mixing rule [44] :

$$18 \quad \Omega^{(l,s)} = \sqrt{(\Omega_{in}^{(l,s)})^2 + (\Omega_{ec}^{(l,s)})^2} \quad (32)$$

19 where the subscripts in and el denote the collision integrals derived from the inelastic and the elastic
 20 interactions, respectively.

21 The charge-exchange cross-section for collisions between unlike species (e.g. $Y^\pm + X \rightarrow X^\pm + Y$) is
 22 small compared to the elastic collision cross-sections and is neglected in this paper. Collision integrals with
 23 even values of l are wholly determined by the elastic interactions.

24 The cross section data required for the determination of the transport coefficients are from a compilation
 25 of data sources as reported in our previous work [18]. Tables 2 is a summary of the methods that are used to
 26 compute the collision integrals for neutral-neutral, neutral-ion and electron-neutral interactions. Interactions
 27 between charged species are described by Coulomb potential screened with the Debye length by charged
 28 particles. The effective collision integrals for charged particles are calculated from the work of Mason et al.
 29 [45]-[46] where the Debye length is calculated considering the contributions from ions and electrons.

1 Table 2 Methods used in the computation of collision integrals.

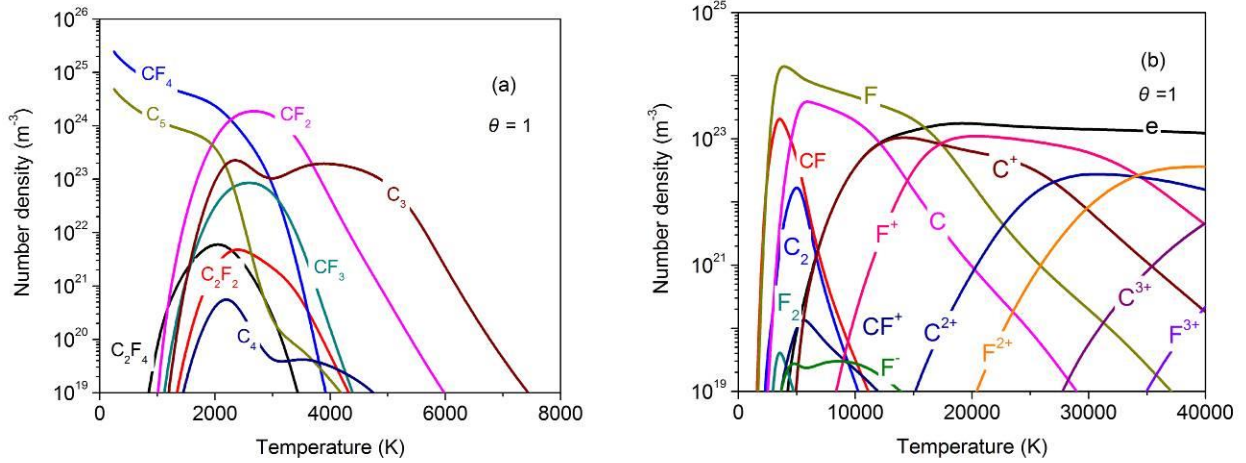
Interaction	Method	Interaction	Method
CF ₄ -CF ₄	Hartree-Fock-dispersion-B potential	C-C	Tabulated collision integrals
F-F	Exponential Repulsive potential and Murrell-Sorbie potential for the repulsive and attractive states	Other neutrals interactions	Phenomenological potential
C-C ⁺ elastic	Hulburt-Hirschfelder potential and Murrell-Sorbie potential	C-C ⁺ inelastic	Integration of transport cross sections
F-F ⁺ elastic	Exponential Repulsive potential and Murrell-Sorbie potential for the unbound and bound states	F-F ⁺ inelastic	Integration of transport cross sections
F-F ⁻ elastic	Exponential Repulsive potential and Murrell-Sorbie potential for the unbound and bound states	F-F ⁻ inelastic	Integration of transport cross sections
F-C ⁻ elastic	Exponential Repulsive potential and Murrell-Sorbie potential for the unbound and bound states	F-C ⁻ inelastic	Integration of transport cross sections
C-F ⁻ elastic	Exponential Repulsive potential and Murrell-Sorbie potential for the unbound and bound states	C-F ⁻ inelastic	Integration of transport cross sections
Elastic involving C ₂ F ⁺ , C ₂ F ⁻ , C ₂ F ₂ ⁻ and F ⁺⁺	Polarization potential	C-C ⁻ inelastic	Integration of transport cross sections
Elastic involving other neutrals and ions	Phenomenological potential	Electron-neutral interaction	Integration of transport cross sections
Charged species interaction	Coulomb potential		

2

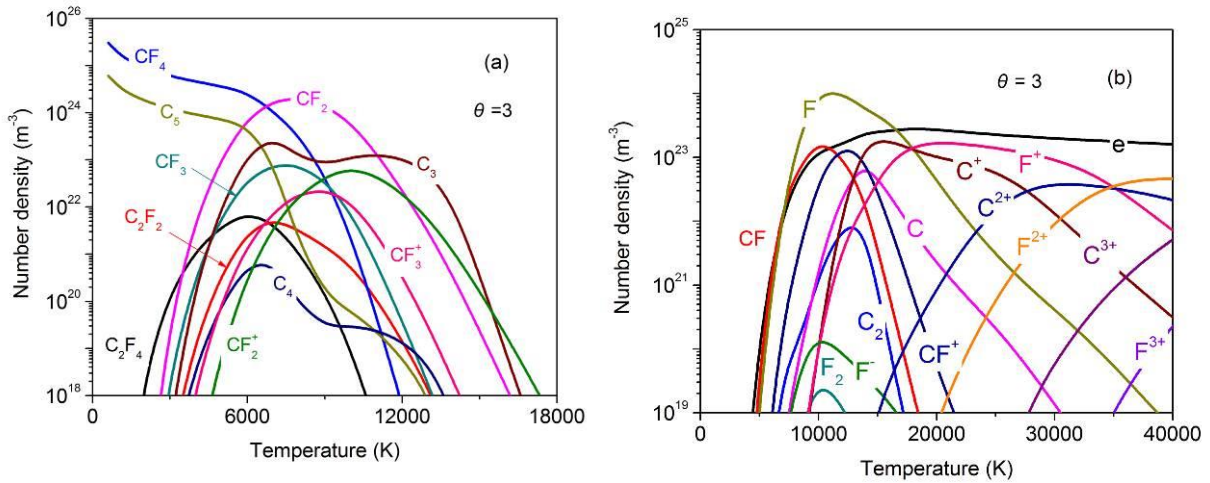
3 3. Results and Discussions

4 Calculated results of species composition, thermodynamic and transport properties over a typical range of
 5 temperature are given at atmospheric pressure. The electron temperature varies from as low as room
 6 temperature up to 40,000 K. The validity of the results is discussed based on comparison with existing results.

7 3.1 Species Composition



1
2 Figure 1 Number density of different species as a function of electron temperature in PTFE plasmas
3 under LTE condition at atmospheric pressure. (a) polyatomic species; (b) monatomic and diatomic species.

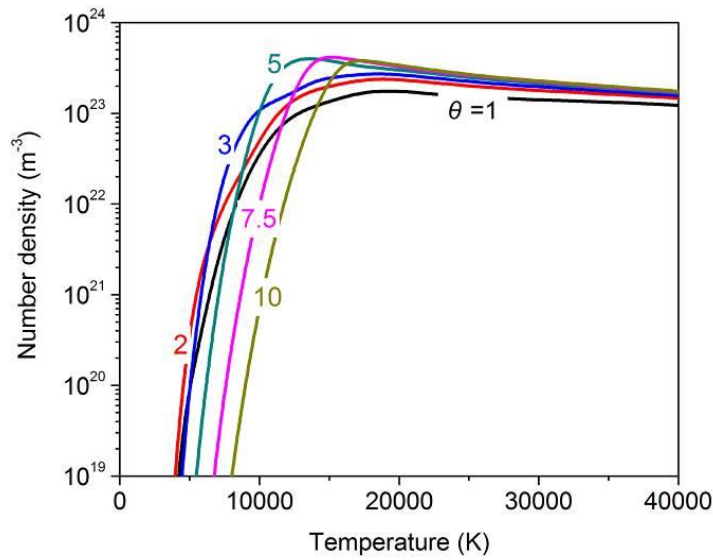


4
5 Figure 2 Number density of different species as a function of electron temperature in PTFE plasmas
6 under a non-equilibrium degree of 3 at atmospheric pressure. (a) polyatomic species; (b) monatomic and
7 diatomic species.

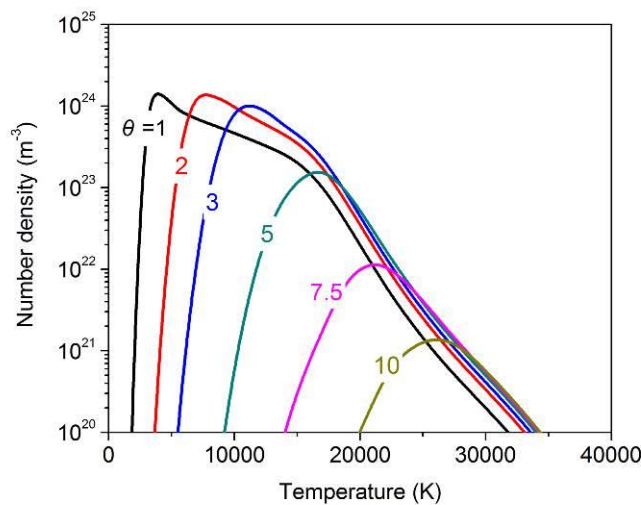
8 The species composition of PTFE plasmas at atmospheric pressure is presented in Figs.1 and 2 as a
9 function of electron temperature under equilibrium and non-equilibrium conditions. At equilibrium ($\theta = 1$),
10 molecules (CF_4 and C_5) collectively dominate the composition up to 2,000 K (Fig.1a). Their dominance is first
11 taken over by CF_2 at 2,200 K when CF_4 starts to rapidly dissociate into CF_3 , CF_2 as well as atomic fluorine.
12 Meanwhile the dissociation of C_5 into C_4 as well as C_3 takes place at around 2,200 K. The dissociation of CF_4 ,
13 with CF_3 and CF_2 as intermediate products, gives rise to rapid increase in the number density of F which
14 becomes the most abundant species between 3,200 K and 16,000 K (Fig.1b). The concentration of atomic
15 carbon also increases as a result of the continuous dissociation of carbon molecules. The ionisation of carbon
16 atoms occurs at a relatively lower temperature around 12,500 K because of its lower ionisation potential
17 (11.20 eV) than that of fluorine atoms (17.4 eV) which starts to be ionised at around 17,500 K. The ionisation
18 reactions keep the electron number density continuously increase until 20,000K with atomic fluorine ions
19 becoming the dominant heavy species in the plasma. With further increase of the temperature, the second and

1 third ionisation of carbon and fluorine occur. Thus to simply the situation in the analysis of the behavioral
 2 patterns of the LTE plasma, It is expected that the gas properties are dominated by (CF_4+CF_2) , F, and
 3 $(F^++electron)$ pairs for temperature up to 4,000 K, 16,000 K and 30,000 K, respectively.

4 When non-equilibrium develops in the PTFE vapor plasma, the dissociation reactions, which are
 5 governed by the heavy particle temperature, are shifted towards a higher electron temperature depending on
 6 the non-equilibrium degree. An example is given in Fig. 2a for the non-equilibrium degree of 3. It is clear that
 7 the molecular ions CF_3^+ , CF_2^+ and CF^+ , which are negligibly small in the LTE case, have a higher
 8 concentration. This is a result of the delayed dissociation and molecular ionisation by more energetic electrons
 9 in the non-LTE case. The plasma composition above 18,000 K is hardly affected the non-equilibrium state
 10 since above this electron temperature, electrons and ions completely dominate the plasma composition. This
 11 can be easily seen by comparing the results in Fig. 1b and 2b.



12
 13 Figure 3 Electrons number density in PTFE plasmas under different non-equilibrium degrees at
 14 atmospheric pressure.



15
 16 Figure 4 Number density of fluorine atoms in PTFE plasmas under different non-equilibrium degrees at

1 atmospheric pressure.

2 Variations of the number density of electrons and fluorine atoms as a function of electron temperature are
3 presented in Figs. 3 and 4 at different non-equilibrium degrees. In the electron temperature range below
4 22,500 K, the electron number density experiences a peak. With an increasing non-equilibrium degree, the
5 number density of electrons grows at an increasing rate with respect to temperature (Figure 3) before reaching
6 its peak value. For $T_e/T_h > 5$ there is apparent shift of the fast rising part of the curve towards high electron
7 temperature. This is because dissociation reactions producing CF_3 , CF_2 and CF as well as atoms are controlled
8 by the heavy particle temperature. To achieve a certain heavy particle temperature, it requires an increased
9 electron temperature when T_e/T_h increases. As a result, the ionization reactions which are controlled by the
10 electron temperature are delayed until the dissociations occur.

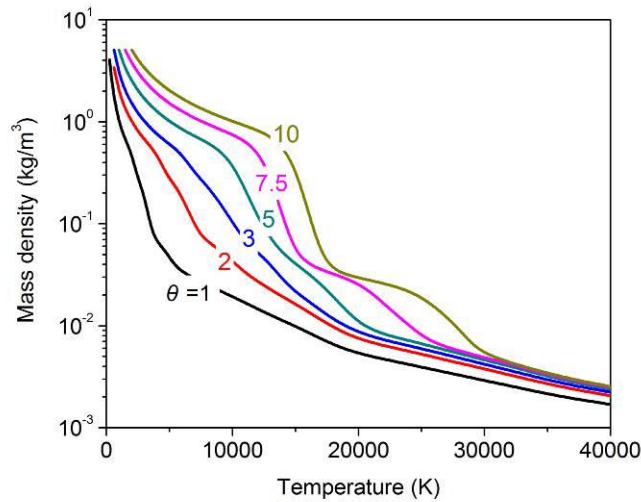
11 It is also clear that a higher electron number density can be obtained in the non-LTE cases. On the one
12 hand, electrons depends on ionisation reactions, as described above. On the other hand, with a higher
13 non-equilibrium degree, there are more high energy electrons for ionisation and there are more molecules or
14 atoms in a unit volume of space to be ionised. The concurrency of these two conditions allows a higher
15 electron number density to be generated. There are three important features in the change of the number
16 density of atomic fluorine, controlled by dissociation (as a generation mechanism) and ionisation (as a loss
17 mechanism).

18 ○Firstly, in equilibrium electron temperature and heavy particle temperature are equal and dissociations
19 reactions leading to the generation of atomic fluorine at low electron temperature (2,200 K) where
20 ionisation is weak. Thus dissociation results in a high peak value of fluorine atom number density.
21 When the non-equilibrium degree is high, such as $T_e/T_h = 5$, at the same heavy particle temperature of
22 22,00 K for dissociation, the electron temperature will be 11,000 K (Figure 4). Due to this ratio of 5, the
23 electron temperature range over which rapid increase of fluorine atom number density takes place is
24 also expanded by about 5 times.

25 ○Secondly, the peak values of the number density of fluorine atom decreases when the non-equilibrium
26 degree increases. This is a direct result of enhanced ionisation due to increased electron temperature
27 during the dissociation stage. The generation rate of fluorine atoms by dissociation reactions is balanced
28 by electron impact ionisation at an earlier stage of the dissociation period thus reducing the highest
29 number density.

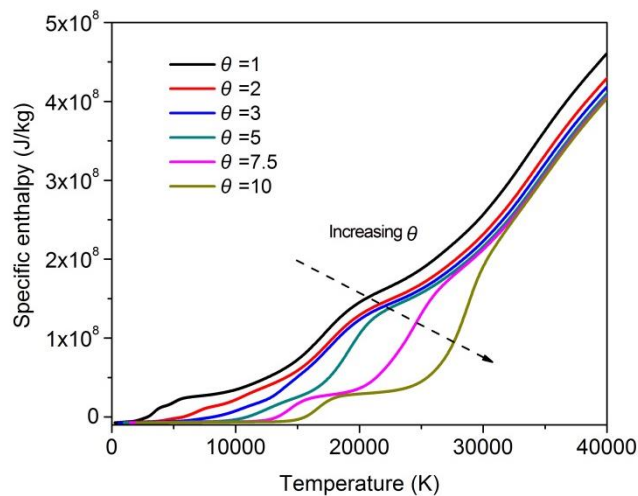
30 ○Once the number density of fluorine atoms reaches its maximum value, the decaying profile curves
31 follow a similar track, especially for those with $T_e/T_h > 2$. This implies that once ionisation of the
32 fluorine atoms by electron impact overtakes dissociative generation of the fluorine atoms, its number
33 density change with respect to electron temperature is affected by heavy particle temperature at a
34 reduced extent. This reduced extent becomes more and more significant so that for $T_e/T_h > 5$ the
35 decaying curves become indistinguishable.

1 3.2 Thermodynamic properties



2
3 Figure 5 Mass density of PTFE plasmas under different non-equilibrium degrees at atmospheric pressure.

4 The mass density of PTFE plasmas with different values of non-equilibrium degree is given in figure 5.
5 The mass density increases at a fixed electron temperature as the θ value rises due to delayed dissociation and
6 ionization. The steepest slope for higher non-equilibrium degree cases ($T_e/T_h > 5$) can be explained by the
7 rapid decrease in the number of heavy molecular weight particles by dissociation and the ionization which is
8 controlled by the heavy particle temperature and electron temperature respectively.

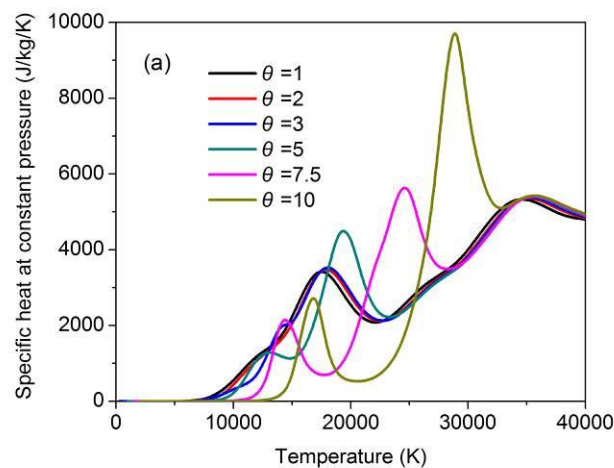


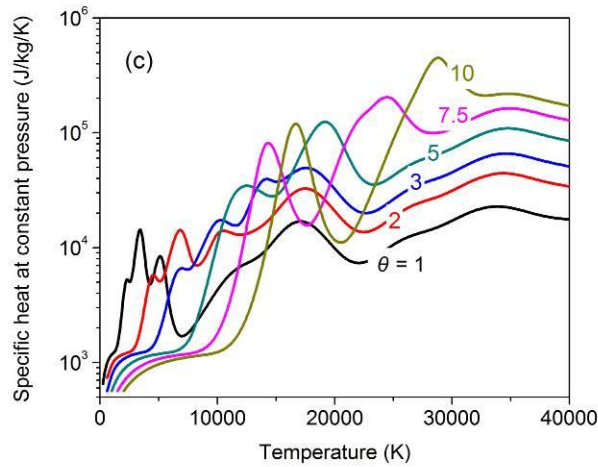
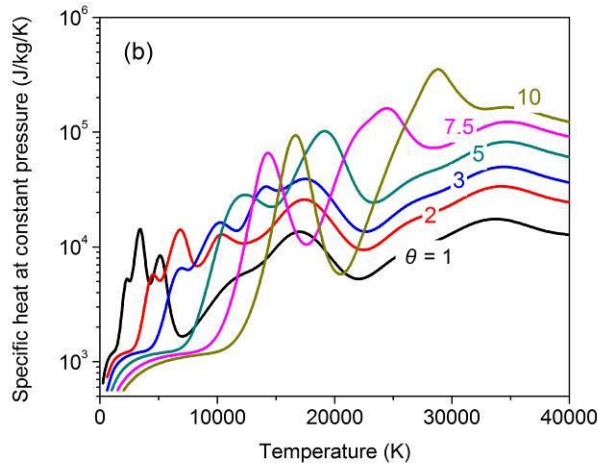
9
10 Figure 6 Specific enthalpy of PTFE plasmas under different non-equilibrium degrees at atmospheric
11 pressure.

12 The specific enthalpy results are given in figure 6 for PTFE plasmas to show its dependence on the
13 non-equilibrium degree. The change in specific enthalpy profile is mainly attributed to the chemical reactions
14 and mass density (see equations (4)-(6)). When θ increases, dissociation is increasingly delayed, resulting in a
15 slowly increasing of specific enthalpy with respect to electron temperature. The occurrence of dissociation and
16 ionisation over a narrower electron temperature range leads to the rapid increase of the specific enthalpy.
17 Moreover, the specific enthalpy decreases with increasing θ values at a given electron temperature. When

1 dissociation is completed (at a higher electron temperature when θ increases), the specific enthalpy becomes
2 only weakly dependent on the non-equilibrium degree.

3 The specific heat as function of electron temperature strongly depends on the non-equilibrium degree as
4 presented in figure 7. For each of the curves the peak at lower temperature corresponds to dissociation and
5 those at higher temperature correspond to ionization, as summarised in Table 1. The peaks in the specific heat
6 curves reflect the rapid change in the specific enthalpy curves. Indeed, the behaviour of electrons' specific
7 heat at constant pressure is closely related to the variation of electron number density and a peak is produced
8 each time a type of ionization takes place. Under thermal equilibrium condition, the peaks of electron specific
9 heat at around 12,500 K, 17,500 K, 27,500 K and 34,000 K correspond to the first and second ionisation of
10 atomic carbon and fluorine respectively. When thermal non-equilibrium exists, molecular ionization also
11 contributes to the peaks of electrons specific heat. For example, for the value of $\theta = 10$, molecular ionization
12 of CF_2 and CF makes significant contribution towards the peaks of electron specific heat at the electron
13 temperatures around 17,500 K and 28,000 K. For heavy particle specific heat, when the non-equilibrium
14 degree is lower than 2, the peaks are, respectively, contributed by the multiple dissociations of CF_4 and C_5 as
15 well as the multiple ionizations of monatomic specie. For the value of $\theta \geq 2$, it is difficult to separate the
16 different contributions; the dissociation and ionization contributions are superimposed. A cross check among
17 the influencing factors show that when sufficiently high electron temperature is reached in the high θ cases,
18 dissociation reactions which are controlled by the heavy particle temperature do not yet generate enough
19 reactants for the ionisation reactions. Once dissociation temperatures are reached, products of molecules and
20 atoms generated by dissociation are immediately ionised. The concurrent dissociation and ionisation processes
21 give rise to an extremely high peak of the specific heat curve. Molecular ionization, which is negligible in
22 thermal equilibrium plasmas, plays an increasing role in the specific heat of the plasma when the
23 non-equilibrium degree becomes high. This is because molecules mainly CF_3 , CF_2 and CF from dissociation
24 are ionised due to high electron temperature before they further dissociate into smaller molecules or atoms
25 under the control of the heavy particle temperature. Comparing results in Figures 7b and 7c, it is evident that
26 heavy particles play a more important role in determining the total specific heat at constant pressure.





1

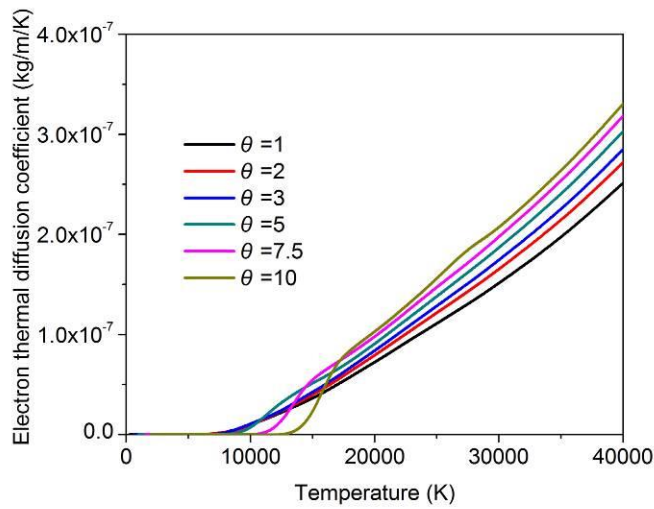
2

3 Figure 7 Specific heat of PTFE plasmas under different non-equilibrium degrees at atmospheric pressure

4 (a) CP_e (b) CP_h (c) CP_t

5 **3.3 Transport Coefficients**

6 **3.3.1 Diffusion coefficients**



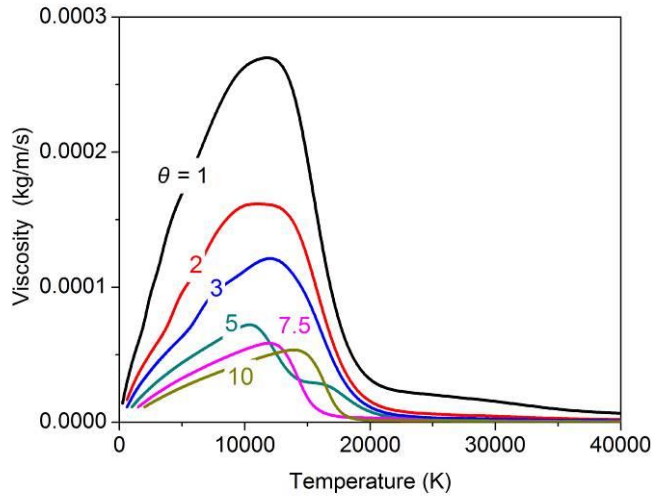
7

8 Figure 8 Electron thermal diffusion coefficient of PTFE plasmas under different non-equilibrium degrees

9 at atmospheric pressure.

1 The electron thermal diffusion coefficient heavily depends on the electron number density and
 2 temperature, as shown in Figure 8. Since ionisation reaction takes place at higher electron temperature with
 3 increasing θ due to the delayed dissociation, this renders a low electron thermal diffusion coefficient for
 4 $T_e < 10,000$ K. As it was shown in Figure 3 that a higher T_e/T_h value in the non-equilibrium case results in a
 5 higher electron number density when $T_e > 15,000$ K, consequently the electron thermal diffusion coefficient
 6 increases with T_e/T_h at a fixed electron temperature.

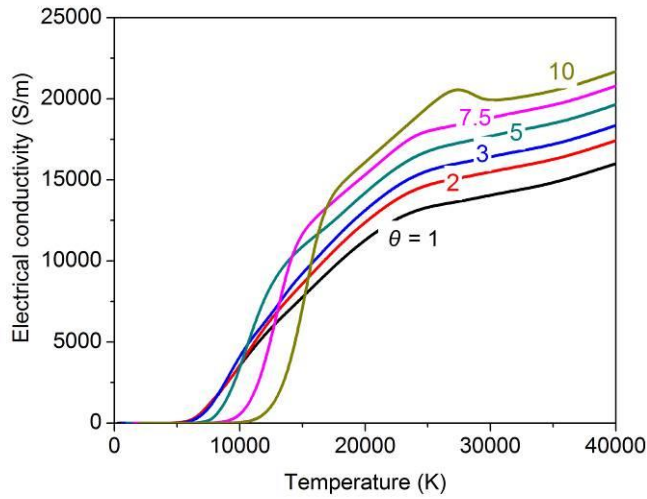
7 3.3.2 Viscosity



8
 9 Figure 9 Viscosity of PTFE plasmas with different non-equilibrium degrees at atmospheric pressure.

10 For all cases with different non-equilibrium degrees, the viscosity first increases with electron
 11 temperature up to $T_e = 10,000$ K when the neutral-neutral collision integrals decrease. It then decreases when
 12 Coulomb interaction, which is stronger than neutral-neutral interaction, starts to dominate. On the other
 13 dimension, when the non-equilibrium degree increases the viscosity peak is reduced and the rate of reduction
 14 with respect to the non-equilibrium degree slows down at higher T_e/T_h . Furthermore the electron temperature
 15 corresponding to the viscosity peak slightly shifts towards higher temperature when T_e/T_h increases.

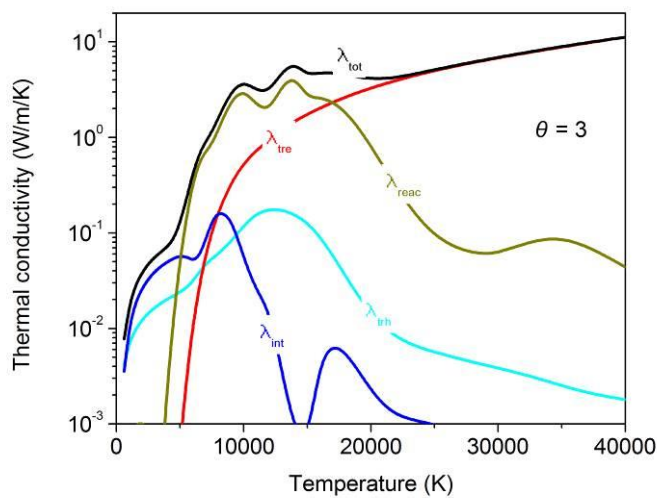
16 3.3.3 Electrical conductivity



1
2 Figure 10 Electrical conductivity of PTFE plasmas with different non-equilibrium degrees at atmospheric
3 pressure.

4 The most significant feature of the electrical conductivity behavior of non-equilibrium plasmas in
5 comparison with the equilibrium case is that it becomes lower than the equilibrium value for a certain
6 temperature range then becomes higher than the latter when electron temperature continues to grow. The
7 lowering of the electrical conductivity is especially manifested in the cases with $T_e/T_h > 5$. It is closely related
8 to the delayed dissociation reactions and the consequent ionizations to produce electrons, as previously
9 discussed (Section 3.3. 1). Dissociation of molecules, which is controlled by heavy particle temperature, does
10 not occur until the corresponding electron temperature is reached. This shifts the ionization towards higher
11 electron temperature as θ increases. Once dissociation starts, the electrical conductivity increases rapidly due
12 to immediate ionization. As clearly shown in Figure 3 the electron number density in logarithm scale increases
13 with T_e/T_h at a fixed T_e for $T_e > 15,000$ K and it is always higher than the equilibrium value. Consequently, the
14 electrical conductivity for $T_e > 15,000$ K is always higher than the equilibrium value and increases with T_e/T_h .

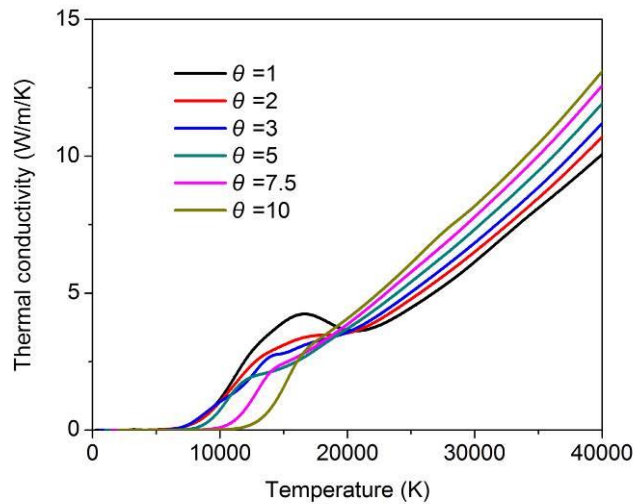
15 3.3.4 Thermal conductivity



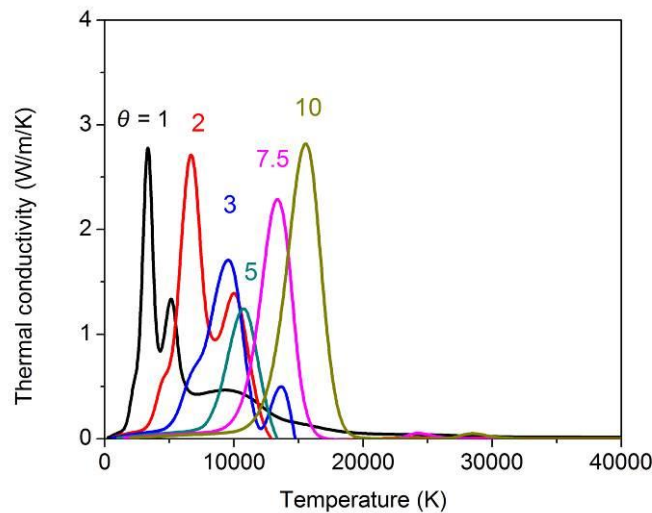
16
17 Figure 11 Different thermal conductivity components of PTFE plasmas with a non-equilibrium degree of

1 3 at atmospheric pressure. λ_{tot} : total thermal conductivity; λ_{trh} and λ_{tre} : translational components due to heavy
 2 particles and electrons respectively; λ_{re} : reactive component; λ_{in} internal component.

3 Different thermal conductivity components of the PTFE plasmas with a non-equilibrium degree of 3 at
 4 atmospheric pressure are presented in figure 11. In the temperature range where dissociation and ionization
 5 take place ($T_e > 5,000$ K), the reactive term makes a major contribution. For electrons, their translational
 6 contribution becomes important in higher temperature range ($T_e > 15,000$ K). For heavy particles, their
 7 translational and internal contribution is only important when $T_e < 5,000$ K. The variation of the total thermal
 8 conductivity for electrons and heavy particles (λ_e, λ_h) is shown in figure 12 and 13, respectively.

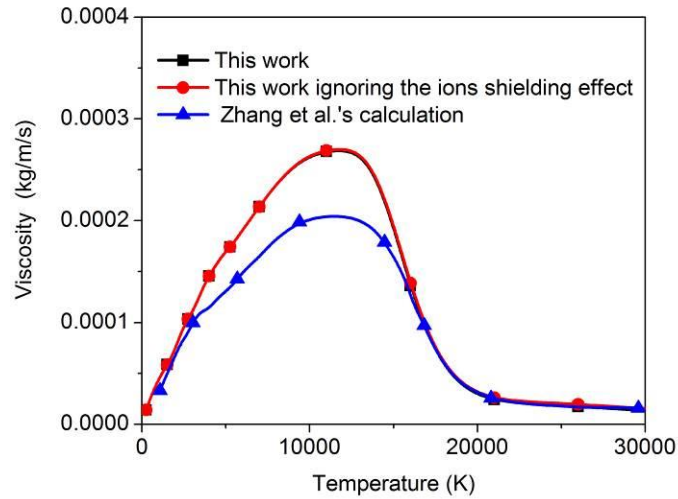


9
 10 Figure 12 Electrons thermal conductivity (λ_e) of PTFE plasmas with different non-equilibrium degrees at
 11 atmospheric pressure.

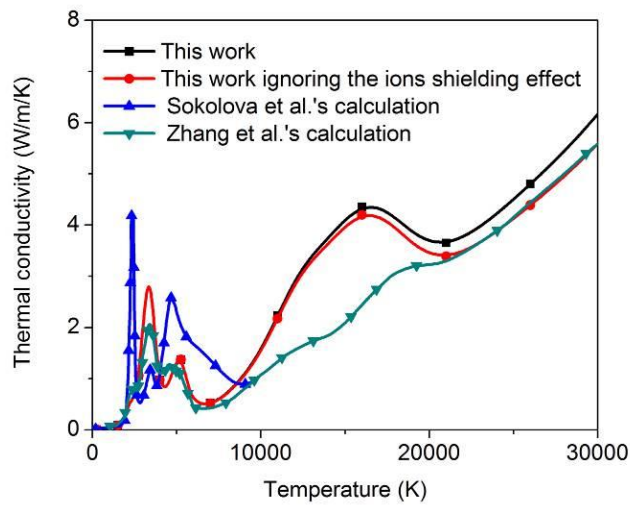


12
 13 Figure 13 Heavy particles thermal conductivity (λ_h) of PTFE plasmas with different non-equilibrium
 14 degrees at atmospheric pressure.

15 **3.4 Comparison with existing data**



(a)



(b)

Figure 14 Comparison of the equilibrium transport coefficients of the PTFE plasma from the present work with those of Zhang et al.[1] and Sokolova et al. [47] at atmospheric pressure (a) viscosity and (b) total thermal conductivity.

From the comparison given in Figure 14 with previously published results, it can be seen that there is large discrepancy at a few temperatures points due to the use of different collision integrals. Our calculated values of viscosity of the PTFE plasma are significantly higher than those calculated by Zhang et al.[1]for temperatures from 3,500K to about 17,500 K. This is attributed to the different interaction potentials used. In their calculation, Lennard–Jones (LJ) potential and polarization potential are used for neutral species and neutral-ion interactions, respectively. These approximate potentials are widely used in the literature due to its ease of computation. However, it has been emphasized that the estimation of the interaction energy from these two classic potentials can be poorly adequate and often brings about large deviation in comparison with the accurate ab initio calculation of interaction potential which uses accurate potential energies and quantum mechanical formulations of scattering and is expected to be more. This can explain our present C-C and F-F interaction results are smaller than those obtained by the Lennard–Jones potential. Although higher values of

1 viscosity collision integrals for C-C⁺ and F-F⁺ interaction from accurate ab initio calculation are adopted in
2 this work, their influences are limited because fluorine atoms can exist with appreciable number density up to
3 high temperature as a result of their high ionization potential. When they begin to be ionized, Coulomb
4 potential starts to dominate due to a high ionization degree of carbon. There exists a large discrepancy of our
5 calculated thermal conductivity with the works of Sokolova et al. [41]. It is possible that some important
6 species with appreciable number density are neglected in Sokolova's calculation. There is generally good
7 agreement with the calculated viscosity of Zhang et al.[1] below 7,000 K although there is some discrepancy
8 in the height of the peaks which, respectively, corresponds to the first ionization of carbon and fluorine atoms.
9 The latter is probably caused by the different charge-exchange cross-section data from different sources used
10 for the atoms and its positive ions.

11 **4. Conclusions**

12 Calculation of the species composition, thermodynamic properties and transport coefficients has been
13 reported in this paper for PTFE vapor plasma at atmospheric pressure but in different degrees of
14 non-equilibrium. The plasma is characterized by the electron temperature (300 to 40,000 K) and the
15 non-equilibrium degree, which is defined as $\theta=T_e/T_h$, under chemical equilibrium. The present work was
16 carried out in order to address the lack of non-equilibrium plasma properties of heated Teflon vapor for the
17 interpretation of experimental results and also for the modelling of the non-equilibrium plasmas.

18 Results show that in comparison with equilibrium cases, the non-equilibrium PTFE plasmas exhibits two
19 important changes, namely the delayed dissociation of polyatomic molecules (also ionization of atomic
20 species) and the increased electron number density. As a result, the non-equilibrium thermodynamic and
21 transport properties show huge difference from the equilibrium values. There are large discrepancies
22 between the present results and those available from published literature (viscosity and thermal conductivity
23 for example). The difference is believed to be associated with the use of different interaction potentials. For
24 the calculation of transport coefficients, the collision integrals used here are expected to be more accurate than
25 previously calculated values; accordingly, results presented in this paper are expected to be more accurate than
26 those previously published.

27 **Acknowledgments**

28 This work was supported by National Natural Science Foundation of China (Grant No. 51407182),
29 Beijing Natural Science Foundation (Grant No. 3154044), the open project of State Key Laboratory of
30 Electrical Insulation and Power Equipment (Grant No.EIPE14208), along with Innovative research fund and
31 Internship project of Qian Xuesen Laboratory of Space Technology.

32 **Reference**

33 [1]Zhang J L, Yan J D, Murphy A B, Hall W and M T C Fang 2002 Computational investigation of arc
34 behavior in an auto-expansion circuit breaker contaminated by ablated nozzle vapor *IEEE Trans. Plasma Sci.*
35 **2** 706–719.

- 1 [2] Paul K C, Sakuta T, Takashima T and Ishikawa M 1997 The dynamic behaviour of wall-stabilized arcs
2 contaminated by Cu and PTFE vapours *J. Phys. D: Appl. Phys.* **30** 103.
- 3 [3] Yang F, Wu Y, Rong M Z, Niu C P 2013 Low-voltage circuit breaker arcs - Simulation and measurements *J.*
4 *Phys. D: Appl. Phys.* **46** 273001.
- 5 [4] Hong D, Dussart R, Cachoncinlle C, Rosenfeld W, Gotze S, Pons J, Viladrosa R, Fleurier C and Pouvesle J
6 M 2000 Study of a fast ablative capillary discharge dedicated to soft x-ray production *REV. of SCIENT. INSTR.*
7 **71** 15-19.
- 8 [5] Schönherr T, Nees F, Arakawa Y, Komurasaki K, and Herdrich G 2013 Characteristics of plasma properties
9 in an ablative pulsed plasma thruster *Phys. Plasmas* **20** 033503.
- 10 [6] Keidar M, Boyd I D, and Beilis I I 2000 Electrical discharge in the Teflon cavity of a coaxial pulsed plasma
11 thruster *IEEE Trans. Plasma Sci.* **28** 376–385.
- 12 [7] Burton R L and Turchi P J 1998 Pulsed Plasma Thruster *Journal of Propulsion and Power* **14** 716-735.
- 13 [8] Kim S H, Yang K S, Lee Y H, Kim J S, and Lee B H 2009 Electrothermal-chemical ignition research on
14 120-mm gun in Korea *IEEE Trans. Magn.* **45** 341–346.
- 15 [9] Keidar M and Boyd I D Ablation study in the capillary discharge of an electrothermal gun 2006 *J. Appl.*
16 *Phys.* 99053 301.
- 17 [10] Autrique D, Gornushkin I, Alexiades V, Chen Z, Bogaerts A, and Rethfeld B 2013 Revisiting the
18 interplay between ablation, collisional and radiative processes during ns-laser ablation *Appl. Phys. Lett.* **103**
19 174102.
- 20 [11] Wang Z B, Hong M H, Lu Y F, Wu D J, Lan B and Chong T C 2003 Femtosecond laser ablation of
21 polytetrafluoroethylene (Teflon) in ambient air *J. Appl. Phys.* **93** 6375.
- 22 [12] Rat V, Murphy A B, Aubreton J, Elchinger M F, and Fauchais P 2008 Treatment of non-equilibrium
23 phenomena in thermal plasma flows *J. Phys. D Appl. Phys.* **41** 183001.
- 24 [13] Wang W Z, Yan J D, Rong M Z, Spencer J W 2013 Theoretical investigation of the decay of an SF₆
25 gas-blast arc using a two-temperature hydrodynamic model *J. Phys. D Appl. Phys.* **46** 065203.
- 26 [14] Wang W Z, Kong L H, Geng J Y, Wei F Z, and Xia G Q 2017 Wall ablation of heated
27 compound-materials into non-equilibrium discharge plasmas *J. Phys. D: Appl. Phys.* **50** 074005.
- 28 [15] Wu Y et al 2016 Calculation of 2-temperature plasma thermos-physical properties considering condensed
29 phases: application to CO₂–CH₄ plasma: part 1. Composition and thermodynamic properties *J. Phys. D: Appl.*
30 *Phys.* **49** 405203.
- 31 [16] Chunping Niu et al 2016 Calculation of 2-temperature plasma thermo-physical properties considering
32 condensed phases: application to CO₂–CH₄ plasma: part 2. Transport coefficients *J. Phys. D: Appl. Phys.* **49**
33 405204.

- 1 [17] Chervy B, Riad H, and Gleizes A Calculation of the interruption capability of SF₆-CF₄ and SF₆-C₂F₆
2 mixtures—Part I: Plasma properties 1996 *IEEE Trans. Plasma Sci.* **24** 198–217.
- 3 [18] Wang W Z, Wu Y, Rong M Z, Éhn L and Černušák I 2012 Thermodynamic properties
4 and transport coefficients of F₂, CF₄, C₂F₂, C₂F₄, C₂F₆, C₃F₆ and C₃F₈ plasmas *J. Phys. D: Appl. Phys.* **45**
5 285201.
- 6 [19] Kovitya P 1984 Thermodynamic and transport properties of ablated vapors of PTFE, Alumina, Perspex and
7 PVC in the temperature range 5,000–30 000 K *IEEE Trans. Plasma Sci.* **PS-12** 38–42.
- 8 [20] Wang W Z, Rong M Z, Wu Y, Spencer J W, Yan J D and Mei D H 2012 Thermodynamic and transport
9 properties of two-temperature SF₆ plasmas *Phys. Plasmas* **19** 3-18.
- 10 [21] Wang W Z, Rong M Z, Yan J D, Murphy A B, and Spencer J W 2011 Thermophysical properties of
11 nitrogen plasmas under thermal equilibrium and non-equilibrium conditions *Phys. Plasmas* **18** 113502.
- 12 [22] van de Sanden M C M, Schram P P J M, Peeters A G, van der Mullen J A M and Kroesen G M W 1989
13 Thermodynamic generalization of the Saha equation for a two-temperature plasma *Phys. Rev. A* **40** 5273-6.
- 14 [23] Wang W Z, Wu Y, Rong M Z, Éhn L and Černušák I 2012 Thermodynamic properties
15 and transport coefficients of F₂, CF₄, C₂F₂, C₂F₄, C₂F₆, C₃F₆ and C₃F₈ plasmas *J. Phys. D: Appl. Phys.* **45**
16 285201.
- 17 [24] Potapov A V 1966 Chemical equilibrium of multi-temperature systems *High Temp.* **4** 48–51.
- 18 [25] van de Sanden M C M, Schram P P J M, Peeters A G, van der Mullen J A M and Kroesen G M W 1989
19 Thermodynamic generalization of the Saha equation for a two-temperature plasma *Phys. Rev. A* **40** 5273-6.
- 20 [26] Wang W Z, Rong M Z, and Spencer J W 2013 Nonuniqueness of two-temperature Guldberg-Waage and
21 Saha equations: Influence on thermophysical properties of SF₆ plasmas *Phys. Plasmas* **20** 113504.
- 22 [27] Gleizes A, Chervy B and Gonzalez J J 1999 Calculation of a two-temperature plasma composition: bases
23 and application to SF₆ *J. Phys. D: Appl. Phys.* **32** 2060–2067.
- 24 [28] Colombo V, Ghedini E and Sanibondi P 2011 Two-temperature thermodynamic and transport properties of
25 carbon–oxygen plasmas *J. Phys. D Appl. Phys.* **20** 035003.
- 26 [29] Ralchenko Y, Kramida A E, Reader J and NIST ASD Team 2008 NIST Atomic Spectra Database (version
27 3.1.5), National Institute of Standards and Technology, Gaithersburg, MD
28 http://physics.nist.gov/PhysRefData/ASD/levels_form.html
- 29 [30] Chase M W, Davies C A, Downey J R, Frurip D J, McDonald R A and Syverud A N 1985 JANAF
30 Thermochemical Tables 3rd edn (Washington, DC: American Chemical Society) *J. Phys. Chem. Ref. Data* **14**
31 1211–60.
- 32 [31] Hirschfelder J O, Curtis C F and Bird R B 1964 *Molecular Theory of Gases and Liquids* 2nd edn (Wiley,
33 New York)

- 1 [32] Chapman S, Cowling T G 1970 *The Mathematical Theory of Non-uniform Gases* 3rd edn (Cambridge
2 University Press, Cambridge)
- 3 [33] Ferziger J H and Kaper H G 1972 *Mathematical Theory of Transport Processes in Gases* (North-Holland,
4 Amsterdam)
- 5 [34] Devoto R S 1967 Third approximation to the viscosity of multicomponent mixtures *Phys. Fluids* **10**
6 2704-06
- 7 [35] Bonnefoi C, Ph.D.thesis, Limoges University, France, 1983.
- 8 [36] Rat V, André P, Aubreton J, Elchinger M F, Fauchais P and Lefort A 2001 Transport properties in a
9 two-temperature plasma: Theory and application *Phys. Rev. E* **64** 26409.
- 10 [37] Colombo V, Ghedini E and Sanibondi P 2009 Two-temperature thermodynamic and transport properties of
11 argon–hydrogen and nitrogen–hydrogen plasmas *J. Phys. D Appl. Phys.* **42** 055213.
- 12 [38] Ghorui S, Heberlein J V R, and Pfender E 2008 Thermodynamic and Transport Properties of
13 Two-Temperature Nitrogen-Oxygen Plasma *Plasma Chem. Plasma Process.* **28**, 553-82.
- 14 [39] Wang W Z, Rong M Z, Yan J D, and Wu Y 2002 The Reactive Thermal Conductivity of Thermal
15 Equilibrium and Nonequilibrium Plasmas: Application to Nitrogen *IEEE Trans. Plasma Sci.* **40** 980-9.
- 16 [40] Ramshaw J D 1993 Hydrodynamic Theory of multicomponent diffusion and thermal diffusion in
17 multitemperature gas mixtures *J. Non-equilib. Thermodyn.* **18** 121-34.
- 18 [41] Ramshaw J D 1996 Simple approximation for thermal diffusion in ionized gas mixtures *J Non-Equilib*
19 *Thermodyn.* **21** 233-8.
- 20 [42] Boulos M I, Fauchais P, and Pfender E, *Thermal Plasmas: Fundamentals and Applications* (Plenum, New
21 York, 1994).
- 22 [43] Laricchiuta A, Bruno D, Capitelli M, Catalfamo C, Celiberto R, Colonna G, Diomede P, Giordano D,
23 Gorse C, Longo S, Pagano D and Pirani F 2009 High temperature Mars atmosphere. Part I: transport cross
24 section *Eur. Phys. J. D* **54** 607–12.
- 25 [44] Murphy A B and Arundell C J 1994 Transport coefficients of argon, nitrogen, oxygen, argon–nitrogen, and
26 argon–oxygen plasmas *Plasma Chem. Plasma Process.* **14** 451-90.
- 27 [45] Mason E A and Munn R J 1967 Transport coefficients of ionized gases *Phys. Fluids* **10** 1827-32.
- 28 [46] Devoto R S 1973 Transport properties of ionized gases *Phys. Fluids* **16** 616-23.
- 29 [47] Sokolova I 2000 High temperature gas and plasma transport properties of F₂ and CF₄ mixtures *Fluid Phase*
30 *Equilib.* **174** 213–20.